The Astrophysical Journal, 616:1204–1214, 2004 December 1

CONSTRAINTS ON PLANETARY COMPANIONS IN THE MAGNIFICATION $A = 256$ MICROLENSING EVENT OGLE-2003-BLG-423[1]

Jaiyul Yoo,[2] D. L. DePoy,[2] A. Gal-Yam,[3,4] B. S. Gaudi,[5] A. Gould,[2] C. Han,[2,6] Y. Lipkin,[7] D. Maoz,[7] E. O. Ofek,[7] B.-G. Park,[8] and R. W. Pogge[2]
(The μFUN Collaboration)

and

M. K. Szymański,[9] A. Udalski,[9] O. Szewczyk,[9] M. Kubiak,[9] K. Żebruń,[9] G. Pietrzyński,[9,10] I. Soszyński,[9] and Ł. Wyrzykowski[7,9]
(The OGLE Collaboration)

Received 2004 March 19; accepted 2004 August 7

ABSTRACT

We develop a new method of modeling microlensing events based on a Monte Carlo simulation that incorporates both a Galactic model and the constraints imposed by the observed characteristics of the event. The method provides an unbiased way to analyze the event, especially when parameters are poorly constrained by the observed light curve. We apply this method to search for planetary companions of the lens in OGLE-2003-BLG-423, whose maximum magnification $A_{\max} = 256 \pm 43$ (or $A_{\max} = 400 \pm 115$ from the light-curve data alone) is the highest among single-lens events ever recorded. The method permits us for the first time to place constraints directly in the planet mass–projected physical separation plane rather than in the mass ratio–Einstein radius plane as was done previously. For example, Jovian-mass companions of main-sequence stars at 2.5 AU are excluded with 80% efficiency.

Subject headings: Galaxy: bulge — gravitational lensing — planetary systems — stars: low-mass, brown dwarfs

1. INTRODUCTION

High-magnification microlensing events are exceptionally sensitive to the presence of planetary companions to the lens. As the projected separation of the source and the (parent star) lens decreases, the size of the images increases, thus enhancing the probability that the planet will pass close enough to an image to generate a noticeable deviation in the light curve (Gould & Loeb 1992). If the source gets sufficiently close to the lens, the light curve can be perturbed by the central caustic associated with the parent star itself (Griest & Safizadeh 1998). Groups that monitor microlensing events to search for planets are well aware of this enhanced sensitivity and so devote special attention to these events.

It is therefore somewhat surprising that the vast majority of events monitored by these groups have not been of particularly high magnification, and the vast majority of the observations of the few that did reach high magnification were actually performed well away from the peak, when the event had far less sensitivity to planets. In particular, of the 43 events monitored by the PLANET collaboration (Albrow et al. 2001; Gaudi et al. 2002) over 5 years, most of the sensitivity to planets came from just five or six events, and most of that from the nearly peak regions of these events. Tsapras et al. (2003) and Snodgrass et al. (2004) used the relatively sparse OGLE data to put limits on planetary systems, although Gaudi & Han (2004) have argued that planets could not be reliably detected from such data alone.

The main reason for this apparent discrepancy was simply a shortage of microlensing alerts. Hence, at any given time, there were just no high-magnification events in progress, or at least none near their peak. The available telescope time then had to be applied to less favorable events. In addition, when devising their observational strategy, PLANET considered that they would have to characterize the events they were monitoring entirely with their own data. Such characterization is absolutely essential to evaluating the sensitivity of each event to planets, and it requires a very large number of observations on the wings and at the baseline, when the event has very little sensitivity to planets.

With the commencement of the OGLE-III project (Udalski et al. 2002), the situation was radically changed. Using its dedicated 1.3 m telescope, large-format ($35' \times 35'$) camera, generally excellent seeing, and ambitious observing strategy, OGLE-III is alerting microlensing events toward the Galactic

[1] Based in part on observations obtained with the 1.3 m Warsaw Telescope at the Las Campanas Observatory of the Carnegie Institution of Washington.

[2] Department of Astronomy, The Ohio State University, 140 West 18th Avenue, Columbus, OH 43210; jaiyul@astronomy.ohio-state.edu, depoy@astronomy.ohio-state.edu, gould@astronomy.ohio-state.edu, pogge@astronomy.ohio-state.edu.

[3] Department of Astronomy, California Institute of Technology, Pasadena, CA 91025; avishay@astro.caltech.edu.

[4] Hubble Fellow.

[5] Harvard-Smithsonian Center for Astrophysics, Cambridge, MA 02138; sgaudi@cfa.harvard.edu.

[6] Department of Physics, Institute for Basic Science Researches, Chungbuk National University, Chongju 361-763, Korea; cheongho@astroph.chungbuk.ac.kr.

[7] School of Physics and Astronomy and Wise Observatory, Tel Aviv University, Tel Aviv 69978, Israel; yiftah@astronomy.ohio-state.edu, dani@astronomy.ohio-state.edu, eran@astronomy.ohio-state.edu, lukas@astronomy.ohio-state.edu.

[8] Korea Astronomy Observatory, 61-1 Whaam-Dong, Youseong-Gu, Daejeon 305-348, Korea; bgpark@boao.re.kr.

[9] Warsaw University Observatory, Al. Ujazdowskie 4, 00-478 Warszawa, Poland; msz@astrouw.edu.pl, udalski@astrouw.edu.pl, szewczyk@astrouw.edu.pl, mk@astrouw.edu.pl, zebrun@astrouw.edu.pl, pietrzyn@astrouw.edu.pl, soszynsk@astrouw.edu.pl, wyrzykow@astrouw.edu.pl.

[10] Departamento de Fisica, Universidad de Concepcion, Casilla 160-C, Concepcion, Chile.

bulge at a rate of 500 per season. Since microlensing events are uniformly distributed in impact parameter u_0 and since peak magnification $A_{\max}$ scales as u_0^{-1} (for $u_0 \ll 1$), this implies that there are dozens of events with $A_{\max} \gtrsim 10$ each year, and a handful with $A_{\max} \gtrsim 100$. Moreover, OGLE-III photometry is publicly available (literally hours after it is taken), so there is generally no need for microlensing follow-up groups to monitor the wings or baseline to characterize the event. That is, follow-up observing time can be concentrated on the highly sensitive peaks of the high-magnification events. In the 2003 season, such peaks were occurring almost continuously. OGLE-III is therefore generating substantial new opportunities for microlensing planet search groups such as PLANET (Albrow et al. 1998), the Microlensing Planet Search (Rhie et al. 1999, 2000), and the Microlensing Follow-Up Network (μFUN; Yoo et al. 2004).

However, the OGLE-III approach also generates substantial challenges. To monitor a very large area during the 2002 and 2003 seasons, OGLE-III returned to each field only of order 50 times over the roughly 9 month season. During the long nights around 21 June, when the bulge transits near midnight, the cadence was relatively high, once every two or three nights. But at the edges of bulge season, the rate of return dropped as low as once per week or lower. Hence, some extremely high magnification events appeared quite ordinary on their last observation before peak and then could be recognized for what they were only very close to (or past) their peak. Indeed, it is quite possible that their true nature as high-magnification events could not be recognized at all from the OGLE-III light curve alone. Thus, without additional work, the riches generated by OGLE-III could easily pass unnoticed. Beginning in the 2004 season, OGLE adjusted its strategy to concentrate on a reduced number of fields that have relatively high expected event rates. Hence, it is expected that the problems mentioned above will be mitigated in future seasons.

Here we develop a new method of modeling microlensing events that incorporates both a Galactic model via a Monte Carlo simulation and the constraints imposed by the observed characteristics of the event. We apply this method to the extreme microlensing event (EME) OGLE-2003-BLG-423, which at $A_{\max} \sim 250$ proves to have the highest magnification ever recorded among single-lens events. As such, the event also has the greatest potential sensitivity to planetary companions of the lens, with a substantial probability of detecting even Neptunian-mass planets, whose event timescale would typically be only about 6 hr. This enhanced sensitivity poses special challenges to the analysis because both the form and amplitude of the impact of such small planets on the light curve depend on the relative size of the source compared with the Einstein ring. If this relative size were known, it would be straightforward to calculate its effect. However, since the light curve is consistent with a point source, our information on the source size is limited.

Similarly, using the light-curve data alone, the impact parameter u_0 is measured only to about 30%. If u_0 were known much more precisely (as it often is for events with relatively bright sources), then we would be able to specify with equal precision where in relation to the Einstein ring a planet could be and still avoid detection. With our less perfect knowledge of u_0, however, we must be satisfied with a more probabilistic statement about these locations.

Both of these challenges are likely to be generic to the analysis of EMEs. Because such events occur with low probability, their sources are most likely to be the relatively common main-sequence (MS) stars that normally lie unnoticed in ground-based bulge images but that can briefly leap to prominence in an EME. Since these MS stars are faint and hence small, they most often avoid finite-source effects even in EMEs. Their faintness also induces large photometric errors in the wings of the light curve, the region that must be well measured to accurately determine u_0. For similar reasons, these two challenges are likely to be key issues in the future even more aggressive microlensing experiments that aim to detect Earth-mass planets by either space-based (Bennett & Rhie 2002) or ground-based (B. S. Gaudi et al. 2004, in preparation) observations.

In our analysis, we take as our starting point the method pioneered by Gaudi & Sackett (2000) and Albrow et al. (2000), which was then applied to a much larger sample by Gaudi et al. (2002). However, we improve on this method in several respects. First, we fix the impact parameter u_0 at a series of different values consistent with the event data and evaluate the sensitivity to companions at each u_0. To find the net sensitivity, we must weight each of these outcomes by the relative probability that the actual event had that particular u_0. Second, we determine these relative probabilities not just from the fit to the light-curve data but also by incorporating the results of a Monte Carlo simulation of events toward the actual line of sight. For each trial u_0, we weight the simulated events by how well they reproduce both the observed characteristics of the light curve and the probability that the source has the luminosity inferred from the light curve combined with the Monte Carlo event parameters, as determined from the *Hipparcos* luminosity distribution at the observed color of the source. This method not only allows us to more accurately estimate the planetary sensitivity, but it also permits us to characterize this sensitivity as a function of planet mass and planet-star separation, since each simulated event has a definite lens mass (drawn from the adopted mass function) and definite lens and source distances (and so a definite Einstein radius). In contrast, the original approach of Albrow et al. (2000) yielded sensitivities in terms of two light curve–fit parameters, the planet/star mass ratio and the separation in units of the Einstein radius.

This method would also permit a similarly rigorous statistical treatment of finite-source effects, since each simulated event has a definite ratio of source size to Einstein radius. However, on the basis of Monte Carlo simulations, we show that in the case of OGLE-2003-BLG-423, finite-source effects are negligible.

2. DATA

OGLE-2003-BLG-423 was alerted by the Early Warning System (EWS; Udalski 2003) at UT 7:38, 2003 September 14, almost exactly 24 hr before the peak on $\mathrm{HJD}' \equiv \mathrm{HJD} - 2{,}450{,}000 = 2{,}897.8070$ and less than 5 hr after the triggering observation by the OGLE-III observatory in Las Campanas, Chile. While the automated alert did not itself call any more attention to this event than the other three that were simultaneously alerted, the OGLE Web site[11] immediately affixed an exclamation point to this event, indicating that it was of special interest. Moreover, from the data available at the Web site, one could see that the event was already 3 mag above baseline and rising rapidly. See Albrow (2004) for a Bayesian approach to

[11] See http://www.astrouw.edu.pl/~ogle/ogle3/ews/ews.html.

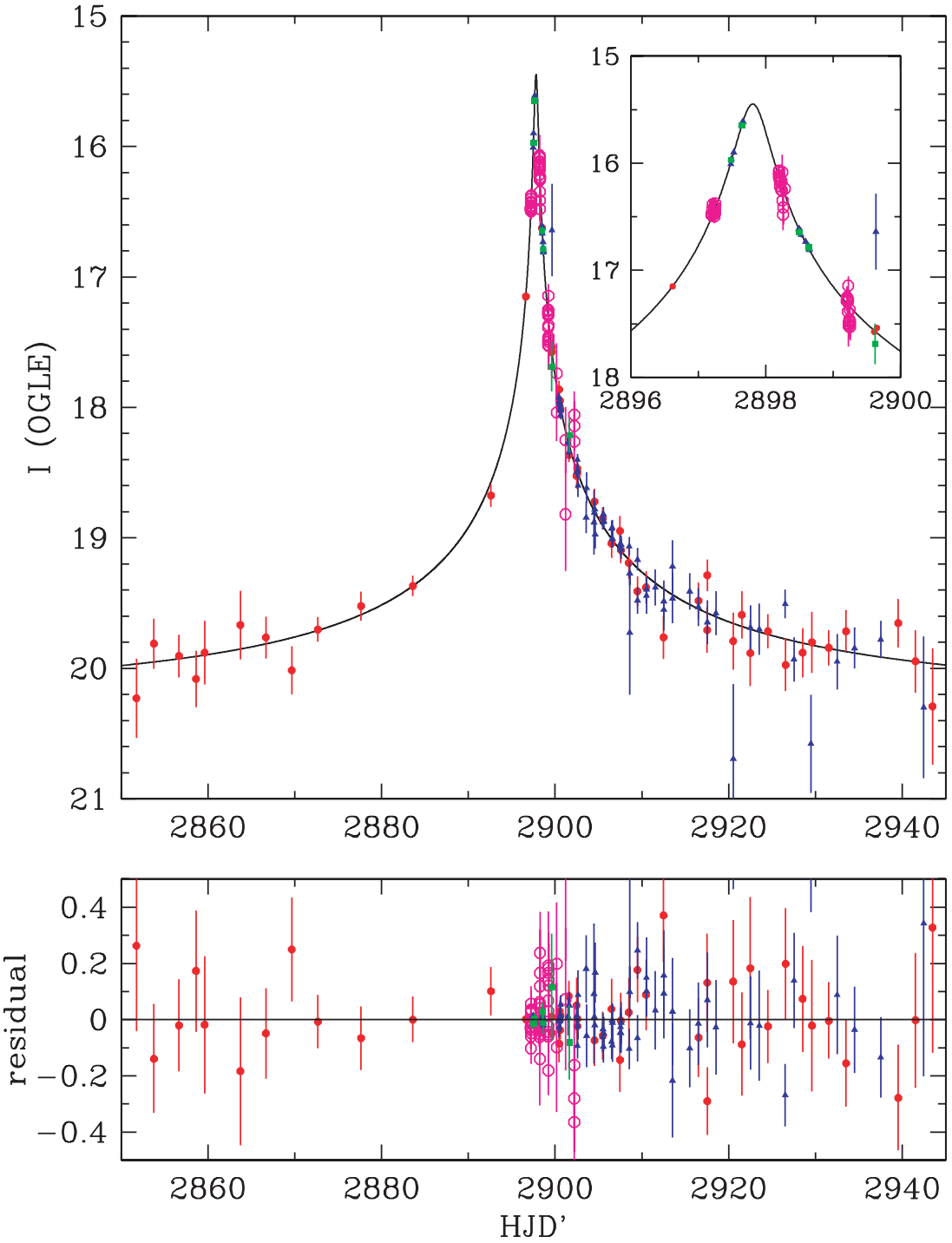

FIG. 1.—Light curve of microlensing event OGLE-2003-BLG-423 near its peak on 2003 September 15 (HJD 2,452,897.8070). Data points with 1 σ error bars are in I (OGLE: *red filled circles*; μFUN Chile: *blue filled triangles*; μFUN Israel: *magenta open circles*) and V (μFUN Chile: *green filled squares*). All bands are linearly rescaled so that F_s and F_b are the same as the OGLE observations, which define the magnitude scale. The solid curve shows the best-fit PSPL model for the I-band curve.

determine whether ascending microlensing events are likely to achieve high magnification.

Immediately following the alert, μFUN decided to focus its observations heavily on this event. Because the event was triggered relatively late in the season, when the bulge was already west of the meridian at twilight, the time per night that it could be observed from any one site was restricted: roughly 1.5 hr from the Wise Observatory in Israel and roughly 4 hr from Cerro Tololo Inter-American Observatory at La Serena, Chile. The gap in coverage between the two observatories was about 6 hr. Because of a communication error, the Chile observations have a gap of 3 hr the first night but are then generally spaced at roughly 1 hr intervals on subsequent nights.

While OGLE-III normally cycles through many fields (survey mode), it can also operate in follow-up mode when there is an event of particular interest. OGLE-2003-BLG-423 was immediately designated as such an event, but because of communication problems, it was not observed the first night following discovery. However, it was observed 1–4 times per night over the next five nights.

When combined, observations from these three observatories provide reasonably good coverage of the peak. See Figure 1.

The μFUN data are available at the μFUN Web site,[12] and the OGLE data are available at the OGLE EWS Web site mentioned above.

From a fit to the first two nights of μFUN observations, it was already clear that the effective timescale of the event was very short, $t_{\rm eff} \equiv u_0 t_{\rm E} = 0.24$ day, where $t_{\rm E}$ is the Einstein crossing time and u_0 is the impact parameter in units of the Einstein radius. Combining this with the Einstein crossing time of $t_{\rm E} = 97$ days derived from the OGLE data yielded an estimate of $A_{\rm max} \simeq 1/u_0 \sim 400$, which would be the highest magnification single-lens event ever recorded. Recognizing the importance of this event, OGLE and μFUN worked together to develop an observation plan that would allow us to characterize it as well as possible. Our principal concern was that if OGLE returned to its regular cycle of observations and μFUN stopped observing the event altogether (as both would normally do several days after the peak), then the OGLE and μFUN observations might barely overlap in time, meaning that the two photometry systems could not be rigidly linked into a single light curve. To resolve this problem, we agreed to observe the event several times for the next few nights (weather permitting) and to continue regularly observing it until it got too close to the Sun.

There are a total of 278 *I*-band images, including 150 from OGLE, 78 from μFUN Chile, and 50 from μFUN Israel. In addition, there are seven *V*-band images from μFUN Chile, all taken near peak to determine the color of the source. Finally, since μFUN Chile observations are carried out with an optical/infrared camera, all *V* and *I* images from this location are automatically accompanied by *H*-band images. However, even at peak, the event was too faint in *H* for these observations to be useful. For each data set, the errors were rescaled to make χ^2 per degree of freedom for the best-fit point-source, point-lens (PSPL) model equal to unity. We then eliminated the largest outlier and repeated the process until there were no 3 σ outliers. This resulted in the elimination of 1 OGLE point, 1 μFUN Chile *I* point, and 1 μFUN *V* point. In the neighborhood of each of these four outliers, there are other data points that agree with the PSPL model, showing that the outliers are indeed caused by systematic errors rather than that they reveal unmodeled structure in the light curve. The final rescaling factors were 1.13 and 0.82 for OGLE and μFUN Chile *I*, respectively. The other two observatory-filter combinations did not require renormalization. The descriptions of the instruments, observing protocol, and reduction procedures are identical to those given in Yoo et al. (2004). The photometry is carried out using the DoPHOT-based PLANET pipeline.

3. POINT-LENS MODELS

The signature of a planetary companion is usually a brief excursion from an otherwise "normal" point-lens magnification light curve. Indeed, as outlined by Gould & Loeb (1992), it is often possible to estimate the planet's properties from the gross characteristics of this deviation. The first step in searching for planets is therefore to fit the light curve to a point-lens model (Albrow et al. 2000). However, planetary deviations can be strongly affected by the finite size of the source, even if the rest of the light curve is perfectly consistent with a point source, which can lead to degeneracies in the interpretation of the deviation (Gaudi & Gould 1997) or even to a complete failure to detect the deviation. Hence, we begin by presenting the best-fit PSPL model and then investigate to what extent finite-source effects can be detected or constrained within the context of point-lens models.

[12] See http://www.astronomy.ohio-state.edu/~microfun.

TABLE 1
OGLE-2003-BLG-423 Fit Parameters

Parameter	Value
Light Curve Alone	
t_0 (days)	2897.8070 ± 0.0030
u_0	0.00250 ± 0.00072
$t_{\rm E}$ (days)	97.4 ± 27.9
$A_{\rm max}$	400 ± 115
I_s	22.0 ± 0.3
$I_{\rm base}$	20.21 ± 0.03
Light Curve and Monte Carlo Simulation	
t_0 (days)	2897.8070 ± 0.0030
u_0	0.00391 ± 0.00066
$t_{\rm E}$ (days)	62.1 ± 10.5
$A_{\rm max}$	256 ± 43
I_s	21.47 ± 43
$I_{\rm base}$	20.21 ± 0.03

3.1. *Point-Source, Point-Lens Model*

We fit the data to PSPL models, defined by three lensing geometric parameters (t_0, u_0, and $t_{\rm E}$), as well as a source flux F_s and a blended-light flux F_b for each observatory-filter combination *i*. That is,

$$F_i(t) = F_{s,i} A(u(t)) + F_{b,i}, \quad A(u) = \frac{u^2+2}{u\sqrt{u^2+4}}, \qquad (1)$$

where $[u(t)]^2 = u_0^2 + (t-t_0)^2/t_{\rm E}^2$. The best-fit parameters and their errors as determined from the light-curve data alone are shown in Table 1 (also see Fig. 1). In Table 2, we present flux parameters from the light curve alone that are rescaled to be the same as in the OGLE *I*-band photometry. We find that even though the event is quite long, the source is too faint to detect microlensing parallax effects.

There are several notable features of this fit. First, the impact parameter is extremely small, $u_0 = 0.00250 \pm 0.00072$, implying that the maximum magnification is $A_{\rm max} = 400 \pm 115$. Second, the source is extremely faint, $I_s = 22.0 \pm 0.3$. The OGLE photometry is not rigorously calibrated but is believed to be accurate to a few tenths. Finally, the errors are quite large, roughly 30% for each of $t_{\rm E}$, u_0, and F_s. In fact, these errors are extremely correlated: appropriate combinations of these parameters, $t_{\rm eff} \equiv u_0 t_{\rm E}$ and $F_{\rm max} \equiv F_s/u_0$, have much smaller errors,

$$t_{\rm eff} = 0.2429 \pm 0.0037 \text{ days}, \quad I_{\rm min} = 15.459 \pm 0.018. \qquad (2)$$

3.2. *Color-Magnitude Diagram*

The first step toward understanding the impact of these measurements and their errors is to place the source on an instrumental color-magnitude diagram (CMD). In Figure 2, we have translated the instrumental CMD to place the clump at $[(V-I)_0,\ I_0] = (1.00,\ 14.32)$, which is the dereddened color and absolute magnitude of the *Hipparcos* (Perryman 1997) clump when placed at the Galactocentric distance, $R_0 = 8$ kpc (Yoo et al. 2004). The source position (as determined from the

TABLE 2
OGLE-2003-BLG-423 Flux Parameters

Parameter	OGLE I	μFUN I Chile	μFUN I Israel	μFUN V Chile
f_s	0.02596	0.02596	0.02596	0.02596
σ_{f_s}	0.00754	0.00745	0.00744	0.00745
f_b	0.10411	0.02396	−0.23491	0.36952
σ_{f_b}	0.00607	0.00484	0.05733	0.08673

Notes.—The parameters are for the light curve alone. The parameter f_s is rescaled to be the same as in the OGLE I photometry.

model fit) is shown as a blue triangle. Since the source is substantially fainter than any of the CMD stars, we also plot the *Hipparcos* lower MS in the figure (also placed at R_0). Note that the source has a dereddened color $(V-I)_0 = 0.73$, almost exactly the same as the Sun. The instrumental source color (and so the source color relative to the clump) is not model dependent: it can be derived directly from a regression of V flux on I flux, without reference to any model. If the source suffers similar extinction as the clump, then the source is about 1.4 mag fainter than the Sun would be if placed at the distance to the clump, i.e., R_0. The Sun is somewhat evolved off the MS, but the source is still more than 1 mag fainter than zero-age MS stars of the same color and metallicity. This offset between the source and the MS (placed at R_0) hardly changes, even if one assumes a substantial difference between the source reddening and the mean reddening toward the clump stars because the reddening vector is nearly parallel to the MS.

There are basically only three effects that could contribute to this offset. First, the source actually could lie well behind the bulge. Second, the source could be relatively metal-poor and thus subluminous compared with solar-neighborhood stars. Third, the microlensing model could be in error, either

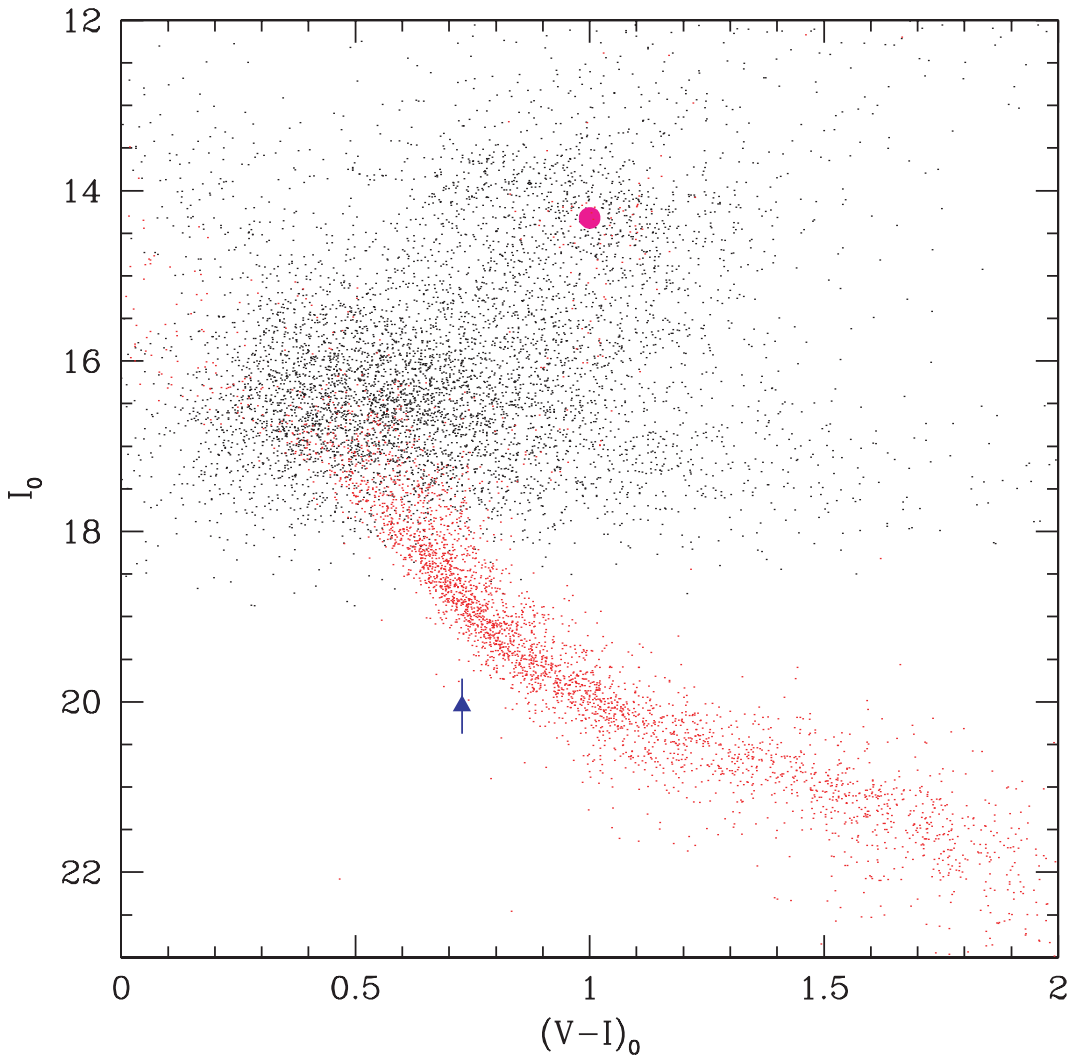

Fig. 2.—Instrumental CMD of a 6′ square around OGLE-2003-BLG-423, which has been converted to dereddened magnitude and color by translating the centroid of the clump giants (*magenta circle*) to its known position $[I_0,\ (V-I)_0]_{\rm clp} = (1.00,\ 14.32)$. *Hipparcos* MS stars placed at $R_0 = 8$ kpc are represented as red points. The source (*blue triangle with 1 σ error bar*) is significantly fainter than the *Hipparcos* stars.

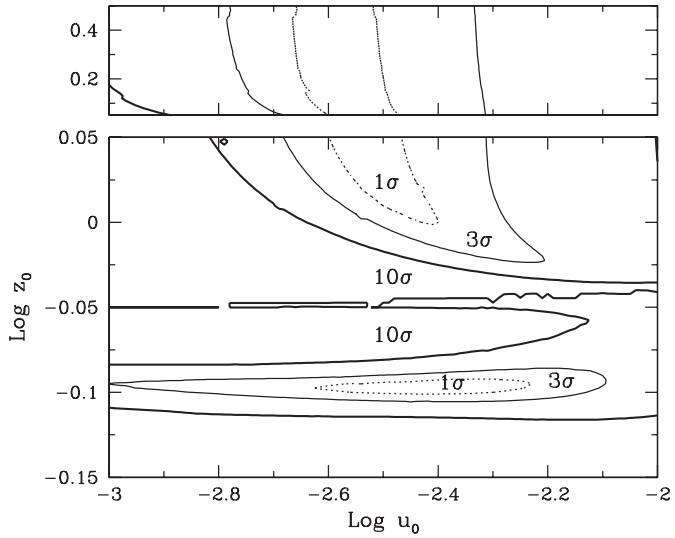

FIG. 3.—Likelihood contours relative to the best-fit PSPL model for various point-lens models with finite-source effects, where u_0 is the impact parameter, $z_0 \equiv u_0/\rho_*$, and ρ_* is the angular size of the source in units of the angular Einstein radius. The two plots are linear in $\log z_0$ but differ in scale. As the source-lens separation increases ($z_0 \gtrsim 1$), the contours become independent of z_0. Note the isolated minimum at $z_0 \simeq 0.8$.

statistically or systematically. We make a more detailed investigation of this offset in § 4.4.

3.3. *Finite-Source Effects*

We now explore a set of models that are constrained to hold u_0 and z_0 at a fixed grid of values. Here $z_0 \equiv u_0/\rho_*$, and $\rho_* = \theta_*/\theta_{\rm E}$ is the angular size of the source θ_* in units of the angular Einstein radius $\theta_{\rm E}$. We take account of limb darkening by parameterizing the surface brightness S by

$$\frac{S(\theta)}{S_0} = 1 - \Gamma\left[1 - \frac{3}{2}(1 - \cos\theta)\right], \tag{3}$$

where θ is the angle between the normal to the stellar surface and the line of sight. Since the source has almost exactly the color of the Sun, we assume solar values for Γ,

$$\Gamma_V = 0.528, \quad \Gamma_I = 0.368. \tag{4}$$

Figure 3 shows the $\Delta\chi^2$ contours for the various models plotted as functions of u_0 and z_0. These contours are essentially independent of z_0 for $z_0 \gtrsim 1$, i.e., for models in which the lens does not pass directly over the source. Note that although models with $z_0 \simeq 1$ are strongly excluded, some models with $z_0 \simeq 0.8$ are permitted at the 1 σ level.

Even though we cannot rule out the model at the isolated minimum ($u_0 \simeq 0.004$ and $z_0 \simeq 0.8$) on the basis of the light-curve data alone, it is extremely unlikely to be able to describe the event if we take account of the observed properties of the event combined with a Galactic model (see § 4). For the moment, we therefore assume $z_0 > 1$ and ignore finite-source effects. Nevertheless, as we describe below, the process of recognizing an EME induces a strong selection bias toward large $t_{\rm E}$ events and thus toward those with high $\theta_{\rm E}$ and/or low relative proper motion μ. Hence, in § 4 we investigate the possibility of $z_0 \lesssim 1$ more closely after we evaluate the posterior probability.

4. MODELING THE EVENT

We first outline a new method to analyze microlensing events that incorporates both a Galactic model via a Monte Carlo simulation and the constraints imposed by the observed characteristics of the event. This method is completely general and can be applied to any microlensing event. We then apply the method to OGLE-2003-BLG-423.

4.1. *General Formalism*

In most scientific experiments, ones seeks to determine the posterior probability $P(\boldsymbol{a}|\Delta)$ of a parameter set $\boldsymbol{a} = (a_1, \ldots, a_n)$ given a data set Δ. By Bayes's theorem,

$$P(\boldsymbol{a}|\Delta) = P_{\rm rel}(\Delta|\boldsymbol{a})P_{\rm pri}(\boldsymbol{a}), \tag{5}$$

where $P_{\rm rel}(\Delta|\boldsymbol{a})$ is the probability of the data given the model parameters $\boldsymbol{a}$ and $P_{\rm pri}(\boldsymbol{a})$ is the prior probability of the parameters. For microlensing events,

$$P_{\rm rel}(\Delta|\boldsymbol{a}_{\rm lc}) = \exp\left(-\Delta\chi^2(\boldsymbol{a}_{\rm lc})/2\right), \tag{6}$$

where $\boldsymbol{a}_{\rm lc}$ is the set of parameters describing the light curve and $\Delta\chi^2(\boldsymbol{a}_{\rm lc})$ is the χ^2 difference relative to the best-fit model.

Since the prior $P_{\rm pri}(\boldsymbol{a}_{\rm lc})$ is often assumed to be uniform, minimization of $\chi^2(\boldsymbol{a}_{\rm lc})$ is the usual method to find a best parameter set $\boldsymbol{a}_{\rm lc}$. This procedure is appropriate when the light curve tightly constrains the parameters, but in general it is more correct to take account of the priors. However, the priors on some of the light-curve parameters $\boldsymbol{a}_{\rm lc}$ cannot be directly specified. While u_0 and t_0 can be taken as random variables drawn from uniform distributions, $t_{\rm E}$ is a function of several independent physical quantities, namely, the lens mass, the distances to the lens and source, and the transverse velocities of the lens and source. We collectively denote these independent physical parameters as $\boldsymbol{a}_{\rm phys}$. Therefore, Bayes's theorem can be rewritten as

$$P\left(\boldsymbol{a}_{\rm lc},\ \boldsymbol{a}_{\rm phys}|\Delta\right) = \exp\left(-\Delta\chi^2(\boldsymbol{a}_{\rm lc})/2\right)P_{\rm pri}\left(\boldsymbol{a}_{\rm lc},\ \boldsymbol{a}_{\rm phys}\right), \tag{7}$$

where it is understood that some of the light-curve parameters are determined by the physical parameters. At the end of the day, one may be more interested in the physical parameters (or some subset of them) than in the light-curve parameters, and so after obtaining the general probability distribution given by equation (7), one may integrate over the remaining "nuisance parameters" to get the probability distribution of a specific physical parameter. Indeed, we do exactly this when we evaluate planet sensitivities in § 6.2.

4.2. *Relative Likelihood*

To apply this general method to OGLE-2003-BLG-423, we first simplify $\Delta\chi^2(\boldsymbol{a}_{\rm lc})$. In principle, $\Delta\chi^2$ is a function of all five parameters, t_0, u_0, $t_{\rm E}$, F_s, and F_b. In practice, t_0 is extremely well determined from the data, while the remaining four parameters are all highly correlated. That is, since $t_{\rm eff} = u_0 t_{\rm E}$ and $F_{\rm max} = F_s/u_0$ (and so $I_{\rm min}$) are very well determined from the light-curve data (see eq. [2]), their product $F_{\rm max}t_{\rm eff} = F_s t_{\rm E}$ is also well determined. Moreover, since the baseline flux is well determined, F_s and F_b are almost perfectly anticorrelated. Hence, once $t_{\rm E}$ is chosen in a particular Monte Carlo realization, I_s is also fixed to within 0.008 mag, and all other

parameters are rigidly fixed as well. Therefore, the relative likelihood is

$$\exp\left(-\Delta\chi^2(\boldsymbol{a}_{\rm lc})/2\right) = \exp\left(-\Delta\chi^2(t_{\rm E})/2\right), \quad (8)$$

where $\Delta\chi^2(t_{\rm E})$ is the χ^2 difference relative to the best-fit PSPL model. Since all the light-curve parameters are determined from the physical parameters via the well-constrained light-curve parameters t_0, $t_{\rm eff}$, and $F_{\rm max}$, Bayes's theorem can be rewritten in our case as

$$P\left(\boldsymbol{a}_{\rm phys}|\Delta\right) = \exp\left(-\Delta\chi^2\left[t_{\rm E}\left(\boldsymbol{a}_{\rm phys}\right)\right]/2\right) P_{\rm pri}\left(\boldsymbol{a}_{\rm phys}\right). \quad (9)$$

4.3. *Prior Probability*

To estimate the prior probability $P_{\rm pri}(\boldsymbol{a}_{\rm phys})$, we apply Monte Carlo realizations to the event, considering all combinations of source and lens distances, $D_l < D_s$, uniformly sampled along the line of sight toward the source $(l,\ b) = (0.^\circ4961,\ -5.^\circ1775)$. We choose a lens mass randomly from the Gould (2000) bulge mass function and use Gaussian random variables to assign each component of the transverse velocities $v_\perp$ of the lens and source. Although this mass function is strictly valid only for the bulge, it should be approximately valid for the disk as well. This is because at $b = -5.^\circ2$, the line of sight generally passes more than a scale height below the Galactic plane, where the stars are older (and therefore more bulge-like) than they are in the immediate solar neighborhood, where the disk mass function is best measured. The event rate for this Monte Carlo realization is then

$$\Gamma \propto \rho_{\rm HG}(D_s) D_s^2 \rho_{\rm HG}(D_l) D_l^2 \theta_{\rm E} \mu, \quad (10)$$

where the density $\rho_{\rm HG}$, as well as the lens and source velocity distribution, are as given by the Han & Gould (1996, 2003) model. The parameters

$$\mu \equiv |\boldsymbol{\mu}_s - \boldsymbol{\mu}_l| = \left|\frac{\boldsymbol{v}_{\perp,s}}{D_s} - \frac{\boldsymbol{v}_{\perp,l}}{D_l}\right|,$$
$$\theta_{\rm E} \equiv \sqrt{\frac{4GM}{c^2}\left(\frac{1}{D_l} - \frac{1}{D_s}\right)}, \quad (11)$$

and $t_{\rm E} = \theta_{\rm E}/\mu$ are all fixed by the chosen distances, transverse velocities, and mass. While this Galactic model is not a perfect representation of the Galaxy, it is substantially more accurate than the uniform prior distribution normally assumed in most microlensing analyses.

We next impose another condition on the prior that constrains $\boldsymbol{a}_{\rm phys}$. Since $t_{\rm E}$ is fixed by the Monte Carlo realization, F_s is also fixed (see § 4.2). By comparing this with the position of the clump on the instrumental CMD, one can then determine the dereddened flux of the source. Since D_s is fixed by the Monte Carlo realization, the absolute magnitude of the source for this Monte Carlo realization can also be inferred. The prior probability is then proportional to N_{Hip}, the number of *Hipparcos* stars with this inferred absolute magnitude (and within 0.02 mag of the measured source $V-I$ color). Hence, if we restrict attention to the kth Monte Carlo realization with physical parameters $\boldsymbol{a}_{{\rm phys},k}$, the prior probability is given by

$$P_{\rm pri}\left(\boldsymbol{a}_{{\rm phys},k}\right) \propto \left(\Gamma N_{Hip}\right)_k. \quad (12)$$

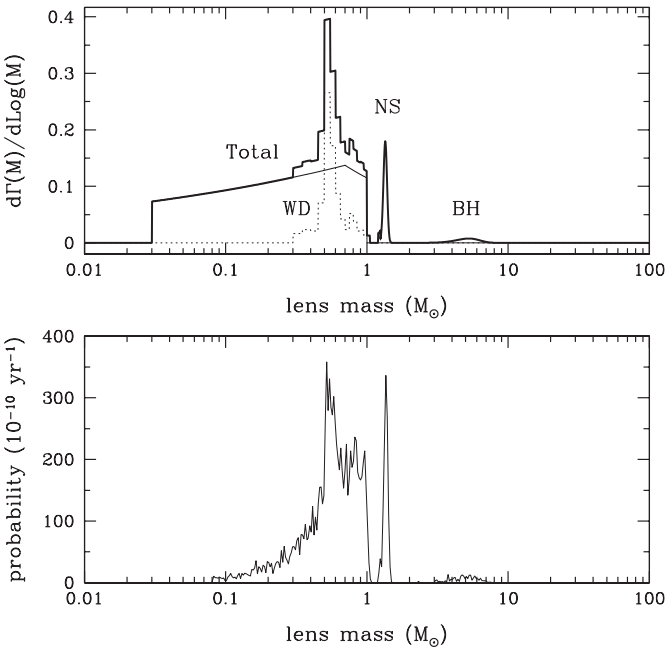

FIG. 4.—Microlensing event rate toward the Galactic bulge as a function of mass. *Top*: Event rates for MS stars and BDs (*thin solid line*) and for white dwarf, neutron star, and black hole remnants (*dotted line*). The total event rate is shown as a thick solid line (see Gould 2000). *Bottom*: Posterior probability of the Monte Carlo events that takes account of both a Galactic model and the *Hipparcos*-based luminosity distribution at the observed source color.

4.4. *Posterior Probability*

Combining equations (9) and (12) implies that the posterior probability that a parameter a_i lies in the interval $a_i \in [a_{i,\rm min},\ a_{i,\rm max}]$ is proportional to

$$P\left(a_i \in \left[a_{i,\rm min},\ a_{i,\rm max}\right]\right) \propto \sum_k P\left(\boldsymbol{a}_{{\rm phys},k}\right), \quad (13)$$

where

$$P\left(\boldsymbol{a}_{{\rm phys},k}\right) = \left(\Gamma N_{Hip}\right)_k \exp\left(-\Delta\chi^2\left(t_{{\rm E},k}\right)/2\right) \times \Theta\left(a_i\left(\boldsymbol{a}_{{\rm phys},k}\right) - a_{i,\rm min}\right) \times \Theta\left(a_{i,\rm max} - a_i\left(\boldsymbol{a}_{{\rm phys},k}\right)\right), \quad (14)$$

a_i is one of the physical parameters $\boldsymbol{a}_{\rm phys}$ (or possibly a function of several physical parameters, as would be the case for $a_i \in \boldsymbol{a}_{\rm lc}$), both $(\Gamma N_{Hip})_k$ and $t_{{\rm E},k}$ are implicit functions of $\boldsymbol{a}_{{\rm phys},k}$, and Θ is a step function.

Letting $a_i = M$, we can evaluate the posterior probability distribution for the lens mass. Figure 4 shows both the event rate Γ and the posterior distribution of microlensing events toward the Galactic bulge as a function of mass. The overall event rate is shown in Figure 4 (*top*). The thin solid and dotted lines represent events from MS stars and brown dwarfs (BDs), and from stellar remnants, respectively. Note that the number of objects in the mass function steeply decreases as the mass increases ($M > 0.7\ M_\odot$) and that in particular there are no MS stars of $M \gtrsim 1\ M_\odot$ in the Galactic bulge, because such stars have already evolved off (Holtzman et al. 1998; Zoccali et al. 2000). However, since the cross section of the microlensing event is proportional to $M^{1/2}$, remnants contribute of order 20% of the bulge microlensing events (Gould 2000). The posterior distribution for the lens mass is shown in Figure 4 (*bottom*).

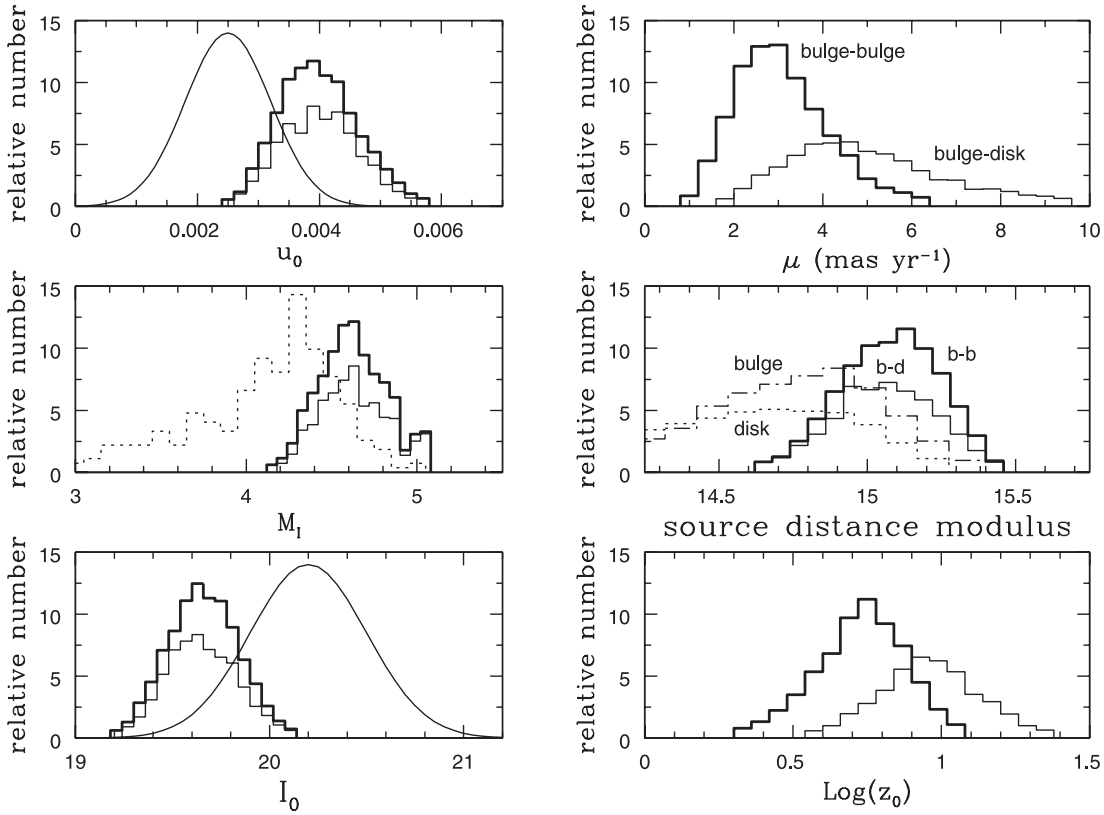

FIG. 5.—Distributions of Monte Carlo microlensing events toward the OGLE-2003-BLG-423 line of sight. The thick and thin solid lines represent bulge-bulge events and bulge-disk events, respectively. The impact parameter, absolute magnitude, dereddened apparent magnitude, and source-lens relative proper motion are denoted u_0, M_I, I_0, and μ, respectively, while $z_0 \equiv u_0/\rho_*$, where ρ_* is the ratio of the source size to the Einstein radius. The Gaussian curves in the u_0 (*top left*) and I_0 (*bottom left*) plots represent the probability distributions derived from the light-curve fit alone, i.e., before applying the constraints from the Galactic model. The dotted histograms in the middle row are the distributions of the *Hipparcos* stars at the color of the source, $(V-I)_0 = 0.73$ (*left*), and lenses in the bulge and disk obtained from a Galactic model alone (*right*).

Note that high masses are strongly favored, possibly because of the long timescale, t_E.

Figure 5 shows the distributions of posterior probabilities of various other parameters. The thick and thin solid histograms represent bulge-bulge and disk-bulge events, respectively. Figure 5 (*top left*) shows the distribution of impact parameters (*histograms*) compared with the distribution derived from the light-curve data alone (*solid curve*). Note that the best-fit u_0 from the light curve alone is somewhat lower than the peak of the posterior distribution (see § 6). The impact parameter and the apparent magnitude are strongly anticorrelated, as is discussed in § 3.1, and Figure 5 (*bottom left*) shows the distribution of source dereddened apparent magnitudes (*histograms*) compared with the distribution based on the light-curve data alone (as represented by the solid curve in Fig. 5 and by the position and error bar in Fig. 2). Taking account of the prior probabilities Γ of the Galactic model and of the M_I distribution of the *Hipparcos* stars at the observed source color $(V-I)_0 = 0.73$ drives the source to somewhat brighter apparent magnitudes, but it is still consistent with the result derived from the light-curve data alone.

The dotted histogram in Figure 5 (*middle left*) represents the absolute magnitude of *Hipparcos* MS stars with the same color as the source. However, the Monte Carlo events favored by the light curve are dimmer than the average *Hipparcos* star at R_0 (see Fig. 5, *middle right*). Figure 5 (*bottom right*) shows the distribution of z_0. As we discuss in § 5, the Monte Carlo realization effectively takes account of the selection effects that push toward low proper motion (and hence lower z_0). Figure 5 (*bottom right*) shows, however, that the probability that z_0 is small enough to generate significant finite-source effects in a point-lens event is extremely small.

The best-fit light-curve parameters and their errors are shown in Table 1. Note that parameters are different at the 2 σ level from those with the light curve alone, and hence, the maximum magnification of the event is $A_{\max} = 256 \pm 43$.

5. INFLUENCE OF SELECTION EFFECTS

As mentioned in § 2, the event was alerted only 24 hr before peak. The observation just prior to this triggering observation was on HJD′ 2892.6, about 4 days before. The event was not alerted from that observation because up to that point there were only two detections on the subtracted images, whereas the alert threshold was set at 3 to avoid spurious events. Even had the event been alerted, it would have been flagged as having an impact parameter of $u_0 = 0.0 \pm 0.2$ and therefore would not have been recognized as a high-magnification event. This 4 day cycle time, which was typical for OGLE-III observations in mid-September, introduces significant selection effects in the recovery of EMEs.

The primary effect is to select for long events. For example, if we consider an event with the same source star, same impact parameter, and same magnification as those on HJD′ 2,892.6 but with t_E shorter by a factor of 2/3, then it would not have been discovered until after peak. That is, such an event would also not have triggered an alert on HJD′ 2,892.6, but at the HJD′ 2,896.6 observation, at which point it would have already been 0.5 days past peak. By the time follow-up observations started, it would have been a day past peak and so would be

magnified only about 40 times. While still impressive, this would not have garnered either the attention or the intensive observations triggered by OGLE-2003-BLG-423.

Thus, the fact that the observed timescale is long compared with that of typical bulge microlensing events is explained largely by selection. However, this selection effect is already fully accounted for in the Monte Carlo realization. Consider a Monte Carlo event that has a $t_{\rm E}$ that is much shorter than the best fit in Table 1, for example, $t_{\rm E} = 20$ days rather than 97 days. To reproduce as well as possible the observed light curve, this event is assigned a source flux that is lower by a factor of $\sim$4.5. In fact, the resulting model light curve reproduces the peak region extremely well: most of the χ^2 difference comes from the postpeak wing, which of course did not enter the selection process. Thus, there is no additional selection discrimination among the Monte Carlo events.

The event appears to have several "abnormal" characteristics relative to typical events as represented in the Monte Carlo realization, and it is of interest to determine which of these are brought about by or enhanced by selection. The most likely source distance is about 2.5 kpc behind the Galactic center. For bulge-bulge lensing, there is a general selection effect driving toward distant sources because these have larger $\theta_{\rm E}$ and thus larger cross sections. See equation (10). However, as shown by the dotted lines in Figure 5 (*middle right*), this effect alone pushes the peak of the distribution back only 1.5 kpc (0.7 kpc for bulge-disk lensing) relative to R_0, not 2.5 kpc. The pressure toward longer events further selects for more distant sources because their larger $\theta_{\rm E}$ values make the events longer. However, since the FWHM of the prior distribution is about 3.5 kpc, the adopted distance would not be extremely unlikely in any case.

Another abnormal characteristic is the faintness of the source. Up to a point, the event selection procedure would appear to pick out brighter sources. As mentioned above, a brighter source would exactly compensate in the selection process for a shorter event, and these are more common than longer events. However, fainter sources are more common than brighter ones, and this is a larger effect. Moreover, as the source brightness increases, so does its angular size, and this eventually cuts off the peak brightness because of finite-source effects. On the basis of Figure 5, however, we have concluded that the source is probably nowhere near this threshold, so this limitation on source size does not enter as a significant factor.

Finally, the source appears to be dim for its color. If the *Hipparcos* distribution is representative of bulge stars of solar color, then this feature would actually be selected against: more luminous stars would be both more numerous and, if lensed by exactly the same lens, more easily recognized before peak. However, it may be that the *Hipparcos* distribution is not representative of the bulge. For example, the stars in the outer bulge may have significantly lower metallicity than those in the solar neighborhood and therefore may be fainter at fixed color, as is true of subdwarfs in the solar neighborhood (e.g., Gould 2004). We conclude that, while a number of the features of this event appear unusual at first sight, most are explained in whole or in part by selection effects.

6. SEARCH FOR PLANETS

6.1. *Detection Efficiency*

As discussed in § 1, Gaudi & Sackett (2000) and Albrow et al. (2000) have already developed a procedure for searching for planets in microlensing light curves, and Gaudi et al. (2002) have applied this to a sample of 43 events. For each event, they considered an ensemble of planetary systems characterized by a planet/star mass ratio q, a planet-star separation (in units of the Einstein radius) d, and an angle α of the source trajectory relative to the planet-star axis. We begin by following this procedure, but we introduce several important modifications.

For a given (d, q), we define the detection efficiency $\epsilon(d, q)$ as the probability that a companion planetary system described by (d, q) would have produced a light-curve deviation inconsistent with the observed OGLE-2003-BLG-423 light curve:

$$\epsilon(d,\ q) = \frac{1}{2\pi}\int_0^{2\pi} d\alpha\ \Theta\left(\chi^2(d,\ q,\ \alpha) - \chi^2_{\rm PSPL} - \Delta\chi^2_{\rm thr}\right), \tag{15}$$

where $\chi^2(d, q, \alpha)$ is the value of χ^2 evaluated for these three parameters, $\chi^2_{\rm PSPL}$ is its best-fit value for the PSPL model, and Θ is a step function. The (d, q) sampling is 0.1 in the logarithm, and the angular step size is set to be $\Delta\alpha = \sqrt{q}/2$ to avoid missing possible planetary perturbations. We choose a conservative threshold, $\Delta\chi^2_{\rm thr} = 60$ (Gaudi et al. 2002). In this incarnation of the procedure, we follow Albrow et al. (2000) and adopt for $\chi^2(d, q, \alpha)$ the minimum value of χ^2 with these three parameters held fixed and all other parameters allowed to vary. The results are shown in Figure 6 (*top*). The curves represent detection efficiencies of 25%, 50%, 75%, and 95%. For $q = 0.1$, companions with separation $0.2 \lesssim d \lesssim 6$ are completely excluded by the data because they would produce deviations $\Delta\chi^2 \equiv \chi^2(d,\ q,\ \alpha) - \chi^2_{\rm PSPL} > 60$ that are not observed. However, the effect of planetary companions of mass ratio $q = 10^{-5}$ would hardly be discernible.

Gaudi et al. (2002) discussed a possible shortcoming of this approach: if (as in the present case) u_0 is not well constrained by the data, then it is possible for the procedure to indicate that certain planetary configurations are permitted by the data when in fact they are excluded. For example, suppose that the measured impact parameter is $u_0 = 0.00250 \pm 0.00072$, while the actual value is $u_0 = 0.003$. For some value of α, the caustic induced by a planet could lie right along the $u_0 = 0.003$ trajectory, but the minimization routine might nevertheless find a path that lies 5 σ ($\Delta\chi^2 = 25$) from this value at $u_0 = 0.006$, thus avoiding the planetary caustic but having $\Delta\chi^2 < 60$ (see Fig. 6 and the accompanying text in Gaudi et al. 2002).

To counter this shortcoming, we evaluate the sensitivity at each allowed value of u_0. Our search of (d, q, u_0) parameter space reveals no planets. The best fit is at $u_0 = 0.002$, $d = 1$, $q = 10^{-3.8}$, but the $\Delta\chi^2$ is only -2.9, far short of our adopted threshold of $\Delta\chi^2_{\rm thr} = -60$. We evaluate the efficiency by modifying equation (15) to

$$\epsilon(d,\ q;\ u_0) = \frac{1}{2\pi}\int_0^{2\pi} d\alpha\ \Theta\left(\chi^2(d,\ q,\ \alpha;\ u_0) - \chi^2_{\rm PSPL}(u_0) - \Delta\chi^2_{\rm thr}\right), \tag{16}$$

where $\chi^2(d, q, \alpha; u_0)$ and $\chi^2_{\rm PSPL}(u_0)$ are now evaluated at a fixed u_0 value. Here u_0 is defined as the projected separation of the source from the center of the caustic induced by the planetary companion. This is the appropriate generalization from the point-lens case, in which u_0 is the projected separation from the (pointlike) caustic at the position of the primary lens.

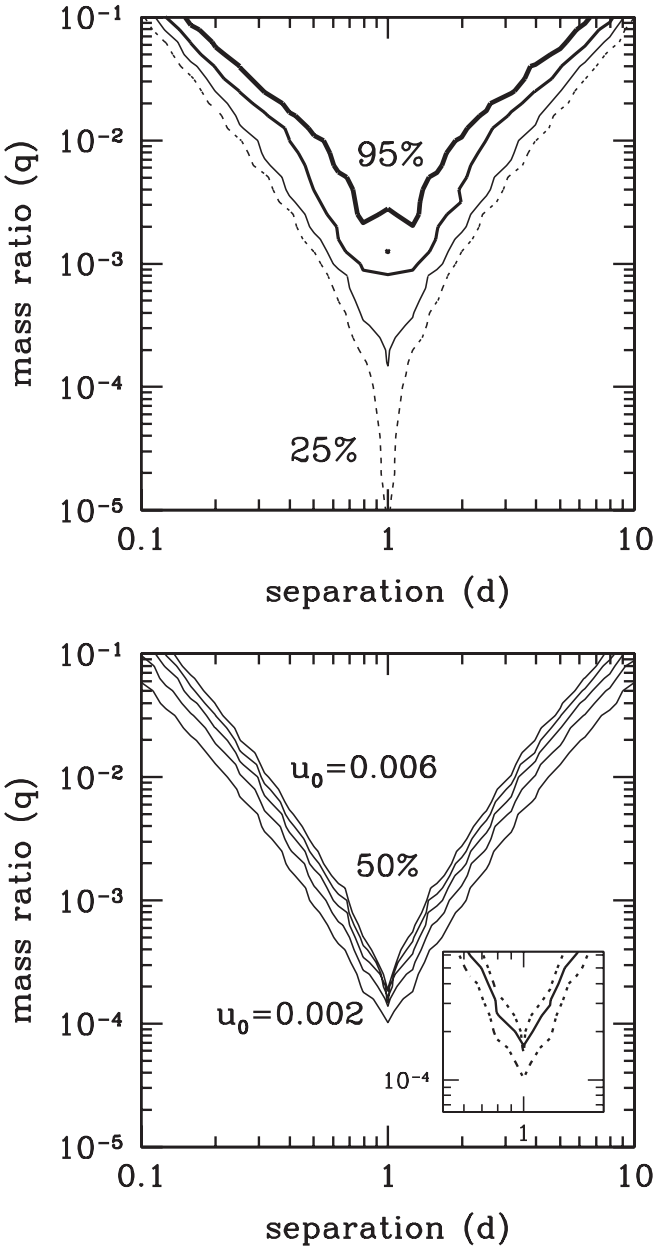

FIG. 6.—Detection efficiency of OGLE-2003-BLG-423 in units of the planet/star mass ratio q and the separation d (normalized to the Einstein radius). *Top*: Detection efficiency contours (25%, 50%, 75%, and 95%) by minimizing χ^2 with respect to t_0, t_E, and u_0 (Albrow et al. 2000). *Bottom*: Contours of 50% efficiency for various fixed u_0 ($u_0 = 0.002$–0.006). As u_0 increases, the efficiency decreases monotonically. *Inset*: For comparison, we present the 50% contours of the former method (*solid line*) and the latter method with $u_0 = 0.002$ and 0.004 (*dashed line*).

Figure 6 (*bottom*) shows 50% contours of detection efficiency for several values of u_0 that are consistent with the Monte Carlo simulation (see Fig. 5). For comparison, we present the 50% contours of the Albrow et al. (2000) method (*inset, solid line*) and of our new method with $u_0 = 0.002$ and 0.004 (*inset, dashed line*). Although the difference is small, we find that the previous method of Albrow et al. (2000) tends to overestimate the detection efficiency.

While it is comforting that the magnitude of this effect is small, its sign is somewhat unsettling. Recall that one motivation for integrating over u_0 rather than minimizing with respect to u_0 was that under the latter procedure, the trajectory could avoid planetary caustics and underestimate the sensitivity. In the present case, however, this effect is outweighed by the fact that the most probable value of u_0 is increased if we take into account the Monte Carlo simulation compared with the fit to the light curve alone. See Figure 5. As discussed in § 1, sensitivity to planets generally decreases with increasing u_0. Note that in this particular case, it is necessary to integrate only over u_0 (and not all light-curve parameters, as originally envisaged by Gaudi et al. 2002) because once u_0 is specified, all the other light-curve parameters are highly constrained (see § 4.2).

One might be concerned about finite-source effects during a planet-caustic crossing. However, we have repeated the calculation including finite-source effects for a variety of (d, q, α) combinations and for various plausible source sizes as determined from Monte Carlo simulations. We find no significant difference in planet detection efficiencies.

6.2. *Constraints on Planets*

Microlensing events provide only degenerate information about physical properties of the source and lens except in so far as other higher order effects, such as finite-source effects and parallax, are detected. However, our new method based on Monte Carlo simulations allows us, for the first time, to break the degeneracy and place constraints on planetary companions in the planet mass–physical separation plane, rather than scaling these quantities to the stellar mass and Einstein radius as was done previously.

For a given ensemble of Monte Carlo events with posterior probabilities $P_k(a_{\rm phys})$, the detection efficiency ϵ can be evaluated as a function of the planet mass m and the planet-star projected physical separation $r_\perp$ by

$$\epsilon(r_\perp,\ m) = \frac{\sum_{k=1}^{N} \epsilon\left(r_\perp/d_{l,k}\theta_{{\rm E},k},\ m/M_k;\ u_{0,k}\right) P\left(a_{{\rm phys},k}\right)}{\sum_{k=1}^{N} P\left(a_{{\rm phys},k}\right)}, \tag{17}$$

where N is the number of Monte Carlo events and $\theta_{\rm E}(M, d_l, d_s)$ is the angular Einstein radius.

Figure 7 shows the resulting detection efficiency; the curves represent the contours for $\epsilon = 25\%$, 50%, 75%, and 95%. Figure 7 shows detection efficiencies for the MS+BDs (*left*) and the remnant stars (*middle*). The total efficiency is shown in Figure 7 (*right*). Since remnant stars are more massive than MS+BDs, at a fixed planet/star mass ratio, microlensing events by remnant stars probe planets of higher absolute mass. Hence, microlensing is less efficient as a probe of planets of remnants than of MS+BDs at a fixed planetary mass.

Because our Galactic model favors substantially lower blending than that implied by the light curve alone, the best-fit magnitude is reduced from $A = 400$ to 256. Nevertheless, OGLE-2003-BLG-423 is the highest magnification single-lens event recorded to date. Despite this honor, the detection efficiency is not quite as good as that of two previous high-magnification events, MACHO-98-BLG-35 ($A_{\rm max} \sim 100$) and OGLE-1999-BUL-35 ($A_{\rm max} \sim 125$) (Gaudi et al. 2002; see also Bond et al. 2002). This is because our observations do not cover the peak of the light curve nearly as densely as was the case in those two events. Peak coverage is the key because the perturbations by planets mostly occur during a small time interval, basically the FWHM around the peak of the event (Rattenbury et al. 2002).

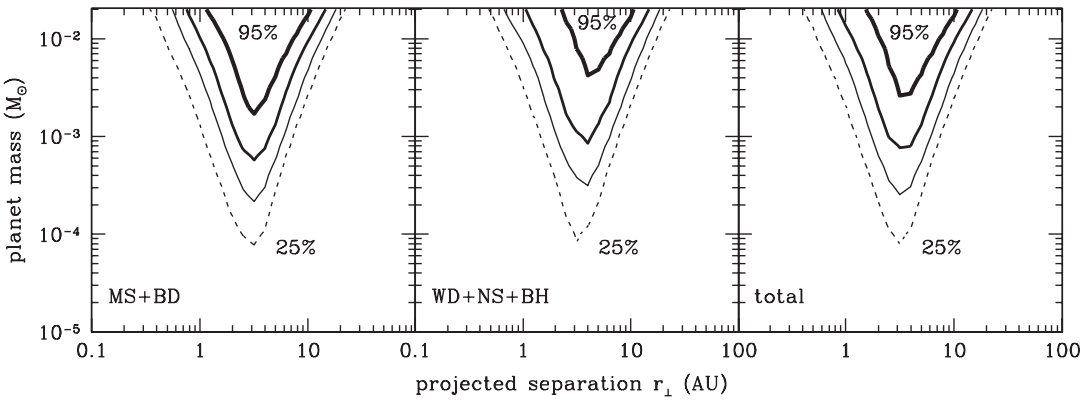

FIG. 7.—Convolved detection efficiency contours of OGLE-2003-BLG-423 as a function of the physical mass and the separation of the planetary companion. The efficiency contours from MS+BDs (*left*) and remnants (*middle*) are shown separately, while the total is shown at right. Contours represent $\epsilon = 25\%$, 50%, 75%, and 95% efficiency.

We thank Jean-Philippe Beaulieu, David Bennett, Martin Dominik, and Phil Yock for valuable comments on the manuscript. Work at Ohio State University was supported by grants AST 02-01266 from the NSF and NAG5-10678 from NASA. A. G.-Y. acknowledges support by NASA through Hubble Fellowship grant HST-HF-01158.01-A awarded by STScI, which is operated by AURA, Inc., for NASA, under contract NAS5-26555. B. S. G. was supported by a Menzel Fellowship from the Harvard College Observatory. C. H. was supported by the Astrophysical Research Center for the Structure and Evolution of the Cosmos (ARCSEC″) of the Korea Science and Engineering Foundation through the Science Research Program. Partial support for the OGLE project was provided with NSF grant AST 02-04908 and NASA grant NAG5-12212 to B. Paczyński and Polish KBN grant 2P03D02124 to A. U. In addition, A. U., I. S., and K. Ż. acknowledge support from the Subsydium Profesorskie grant from the Foundation for Polish Science.

REFERENCES

Albrow, M. D. 2004, ApJ, 607, 821
Albrow, M. D., et al. 1998, ApJ, 509, 687
———. 2000, ApJ, 535, 176
———. 2001, ApJ, 556, L113
Bennett, D. P., & Rhie, S. H. 2002, ApJ, 574, 985
Bond, I. A., et al. 2002, MNRAS, 333, 71
Gaudi, B. S., & Gould, A. 1997, ApJ, 486, 85
Gaudi, B. S., & Han, C. 2004, ApJ, 611, 528
Gaudi, B. S., & Sackett, P. D. 2000, ApJ, 528, 56
Gaudi, B. S., et al. 2002, ApJ, 566, 463
Gould, A. 2000, ApJ, 535, 928
———. 2004, preprint (astro-ph/0403506)
Gould, A., & Loeb, A. 1992, ApJ, 396, 104
Griest, K., & Safizadeh, N. 1998, ApJ, 500, 37
Han, C., & Gould, A. 1996, ApJ, 467, 540
———. 2003, ApJ, 592, 172
Holtzman, J. A., et al. 1998, AJ, 115, 1946
Perryman, M. A. C. 1997, The *Hipparcos* and Tycho Catalogues (SP-1200; Noordwijk: ESA)
Rattenbury, N. J., Bond, I. A., Skuljan, J., & Yock, P. C. M. 2002, MNRAS, 335, 159
Rhie, S. H., Becker, A. C., Bennett, D. P., Fragile, P. C., Johnson, B. R., King, L. J., Peterson, B. A., & Quinn, J. 1999, ApJ, 522, 1037
Rhie, S. H., et al. 2000, ApJ, 533, 378
Snodgrass, C., Horne, K., & Tsapras, Y. 2004, MNRAS, 351, 967
Tsapras, Y., Horne, K., Kane, S., & Carson, R. 2003, MNRAS, 343, 1131
Udalski, A. 2003, Acta Astron., 53, 291
Udalski, A., et al. 2002, Acta Astron., 52, 1
Yoo, J., et al. 2004, ApJ, 603, 139
Zoccali M., et al. 2000, ApJ, 530, 418